Angular distributions of fragments from fission induced by 220-MeV ^{20}Ne on targets of ^{165}Ho, ^{197}Au, and ^{209}Bi

H. Rossner, D. Hilscher, E. Holub,* G. Ingold, U. Jahnke, and H. Orf
Hahn-Meitner-Institut für Kernforschung Berlin, 1000 Berlin 39, Federal Republic of Germany

J. R. Huizenga, J. R. Birkelund, W. U. Schröder, and W. W. Wilcke
Departments of Chemistry and Physics and Nuclear Structure Research Laboratory, University of Rochester, Rochester, New York 14627
(Received 2 November 1982)

Fragment angular distributions are reported for 220-MeV ^{20}Ne induced fission of ^{165}Ho, ^{197}Au, and ^{209}Bi. The experimental anisotropies are underestimated and overestimated, respectively, by calculations using the moments of inertia derived from the rotating and nonrotating ($I=0$) liquid-drop models. Account is taken in the theoretical calculations of both prefission particle emission and incomplete fusion. It is possible to obtain satisfactory fits to the experimental angular distributions with spin dependent values of $\mathcal{I}_{\rm sph}/\mathcal{I}_{\rm eff}(I)$ if the rotating liquid-drop model condition that $\mathcal{I}_{\rm sph}/\mathcal{I}_{\rm eff}(I)$ goes to zero at $I_{\rm RLDM}$ ($B_f=0$) is relaxed. For heavy-ion induced fusion-fission reactions, as l_f exceeds $I_{\rm RLDM}$ and the unconditional saddle-point energy has gone to zero, the saddle-point configuration plays less and less of a role in establishing K_0^2.

NUCLEAR REACTIONS ^{165}Ho, ^{197}Au, ^{209}Bi (^{20}Ne, fusion-fission), $E_{\rm lab}=220$ MeV. Measured fission fragment angular distributions. Theoretical calculations with RLDM and LDM ($I=0$) moments of inertia including prefission particle emission and incomplete fusion.

I. INTRODUCTION

Considerable experimental evidence[1] has shown that nuclei excited to moderate energies and spins fission along their symmetry axis where the projection K of the total angular momentum I on this symmetry axis is a good quantum number. In the transition state model of fission,[2] the angular distribution of fission fragments is completely determined by the quantum numbers I, K, and M, the latter being the projection of I on a space fixed axis. Although K may change continuously during the time evolution of the fusion-fission process, as, for example, in the transition of a triaxial compound nucleus to an axially symmetric transition state, the transition state theory assumes that the K distribution is frozen in at the saddle point and is not altered by the Coriolis forces on the path to scission. At excitation energies well in excess of the fission barrier, it has been shown that the transition state deformation[3] as a function of the fissility parameter X closely follows the liquid-drop[4] saddle-point shapes.

The K distribution of the transition states is usually approximated by a Gaussian centered at $K=0$ with a variance $K_0^2(I)$ given by[1,5]

$$K_0^2(I)=\frac{\mathcal{I}_{\rm sph}}{\hbar^2}\frac{T}{[\mathcal{I}_{\rm sph}/\mathcal{I}_{\rm eff}(I)]}\ , \tag{1}$$

where T is the nuclear temperature at the saddle-point deformation and $\mathcal{I}_{\rm sph}$ is the rigid-body moment of inertia of a sphere. The effective moment of inertia, defined by

$$\mathcal{I}_{\rm eff}(I)=\mathcal{I}_{||}(I)\mathcal{I}_{\perp}(I)/[\mathcal{I}_{\perp}(I)-\mathcal{I}_{||}(I)]\ , \tag{2}$$

determines the magnitude of $K_0^2(I)$, where $\mathcal{I}_{||}(I)$ and $\mathcal{I}_{\perp}(I)$ are the moments of inertia parallel and perpendicular to the nuclear symmetry axis, respectively. For a Gaussian K distribution, the transition state theory predicts (for $M=0$) that the fission fragment angular distribution is given by[1,6]

$$W(\theta) \propto \sum_I (2I+1) T_I \left\{ \frac{\sum_{K=-I}^{I} \frac{1}{2}(2I+1) \left| D^I_{M=0,K}(\theta) \right|^2 \exp\left[-\frac{K^2}{2K_0^2(I)} \right]}{\sum_{K=-I}^{I} \exp\left[-\frac{K^2}{2K_0^2(I)} \right]} \right\}, \tag{3}$$

where the summation extends over all spin values I contributing to fission. In Eq. (3) the transmission coefficients are written as T_I, since $l=I$ when $M=0$. The $D^I_{M,K}(\theta)$ functions are defined and their use described in Ref. 1. Equation (3) is an exact theoretical expression for computation of fission-fragment angular distributions when both target and projectile spins are zero.

The rotating-liquid-drop model[4] (RLDM) predicts that $\mathcal{I}_{\rm sph}/\mathcal{I}_{\rm eff}(I)$ decreases, i.e., that the saddle-point configuration becomes more compact with increasing I, and vanishes at $I_{\rm RLDM}$ where $B_f=0$. In the simple transition-state theory, as $\mathcal{I}_{\rm sph}/\mathcal{I}_{\rm eff}(I)$ approaches zero, $K_0^2(I)$ approaches infinity and the fission fragment angular distribution becomes isotropic. In order to perform a realistic comparison of experimental results with the RLDM, one has to know the fissility parameter, temperature, and spin distribution of the actual fissioning system. Insofar that prefission particle emission can have drastic effects on these parameters, the ^{165}Ho+^{20}Ne reaction is chosen here as a system particularly suited for the above comparison since prefission neutron emission has been studied.[7] Furthermore, a weakly fissile composite system, such as ^{185}Ir ($X=0.663$), samples the K distribution for high angular momenta. This results from the observation that a sizable fraction of the fusion cross section, given by $\sigma_{\rm fus}=\sigma_{\rm ER}+\sigma_{\rm FF}$, is due to evaporation residues (ER). Hence, only the angular momenta in the window between $l_{\rm ER}$ [$\propto(\sigma_{\rm ER})^{1/2}$] and l_f [$\propto(\sigma_{\rm ER}+\sigma_{\rm FF})^{1/2}$] contribute to the fission fragment angular distribution [see Eq. (3)] via the appropriate values of $\mathcal{I}_{\rm eff}(I)$ in the simple RLDM, where only $I<I_{\rm RLDM}$ ($B_f=0$) values contribute to the anisotropy.

It has been known for some time that fusion-fission types of processes occur for heavy systems with a cross section[8] that may considerably exceed the limiting angular momentum $I_{\rm RLDM}$ predicted by the RLDM. Furthermore, fission fragment angular distributions for very heavy nuclei formed by ^{32}S projectiles show large anisotropies,[9] although nearly spherical saddle-point configurations are predicted for these systems by the RLDM. When the combined effects of Coulomb and centrifugal forces become very large, measured "fusion" cross sections deviate markedly from the predictions of a one-dimensional dynamical fusion model[8] based on the proximity formalism.[10,11] Experimentally, fusion for these systems can be described by a recent dynamical model of Swiatecki[12,13] where an "extra push" energy is required to induce fusion.

Equation (1) relates a statistical K distribution with a nuclear shape at the instant when it is determined. For the nonrotating case, the K distribution is frozen in at the saddle-point deformation and it is assumed that K remains a constant of the motion as the system moves toward scission. For a rapidly rotating system the Coriolis forces destroy the axial symmetry and the fissioning system may continue to adjust its K distribution beyond the saddle point. However, at some deformation on the path to scission the K distribution no longer changes significantly and it is this distribution and its associated shape that are determined by fission fragment angular distributions. When the fission barrier has vanished, one can no longer invoke the concepts of compound nucleus formation and unconditional saddle shapes. In this case the projectile and target amalgamate during the inward radial motion, and the composite system eventually leads to symmetric fragmentation. The stage at which the K distribution is frozen in for such systems may be near the turning point of the trajectory, where it spends a considerable fraction of its lifetime. Although such a postulate for the turning point in symmetric fragmentation playing the role of the saddle in compound nucleus reactions is plausible, the K distribution may well be established at a later stage for these systems with large angular momenta. Furthermore, the presence or absence of a small fission barrier may be of little importance in determining where the K distribution is frozen in for rapidly rotating nuclei at high excitation energy.

In addition to the ^{185}Ir ($X=0.663$) system, the more fissile systems ^{217}Ac ($X=0.761$) and ^{229}Np ($X=0.792$), prepared by the ^{197}Au+^{20}Ne and ^{209}Bi+^{20}Ne reactions, respectively, have also been studied. For each of these reactions the evaporation residue cross sections are negligible, and all angular momenta $l \leq l_f$ contribute to the fusion-fission process. Unfortunately, no experimental information is available on the prefission particle emission for either of these systems.

It is the purpose of this paper to enumerate some of the uncertainties involved in a theoretical analysis

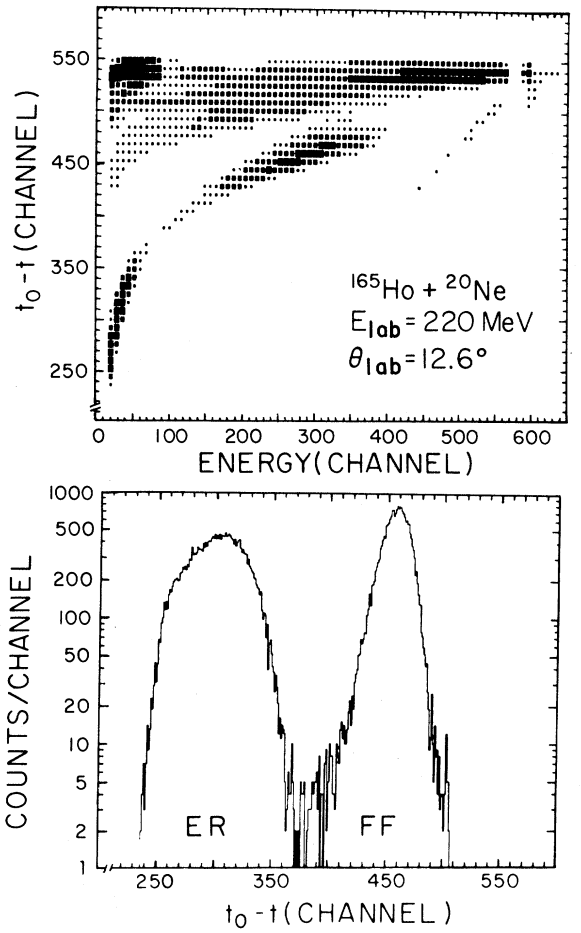

FIG. 1. The upper part shows a plot of the time versus energy spectrum of all reaction products. The events clustered near energy channel 300 and time (t_0-t) channel 450 are fission fragments, and events near energy channel 40 and time (t_0-t) channel 310 are evaporation residues. The lower part shows a gated spectrum of the same data including only the evaporation residue (ER) and fission fragment (FF) intensities projected onto the time (t_0-t) axis.

of heavy-ion experimental fission fragment angular distributions where angular momenta well beyond I_{RLDM} may contribute to the fusion-fission process. Section II gives a short description of the experimental procedure. In Sec. III, theoretical angular distributions based on a number of different functional forms of $K_0^2(I)$ are discussed and compared with the experimental data. These functional forms of $K_0^2(I)$, derived from moments of inertia, have been determined from the RLDM, and its $I=0$ version, referred to as the nonrotating liquid drop model (LDM), and from empirical relations. Finally, available data for rapidly rotating systems are parametrized in terms of $\mathcal{I}_{\mathrm{sph}}/\mathcal{I}_{\mathrm{eff}}(I)$ as a function of the fissility parameter X, where $\mathcal{I}_{\mathrm{eff}}(I)$ is assumed to be constant for all I. Section IV contains conclusions.

II. EXPERIMENTAL PROCEDURE

Angular distributions of fission fragments and evaporation residues induced by 220-MeV ^{20}Ne projectiles on targets of ^{165}Ho, ^{197}Au, and ^{209}Bi were measured with two solid-state detectors positioned on both sides of the beam at 19 and 9 cm from the target for θ_{lab} smaller and larger than 10°, respectively. The apertures in front of the detectors were 2.2 mm in diameter. In order to obtain the fragment masses, the time of flight of the fragments from the target to the detector was measured by utilizing the pulsed-beam facility of the VICKSI accelerator at the Hahn-Meitner-Institut in Berlin. The overall time resolution of this system was 0.5 ns. Typical data are shown in Fig. 1. In the upper part of this figure is plotted a time (t_0-t) versus energy spectrum where the different types of reaction products are clearly separated from one another. The lower part of Fig. 1 illustrates a gated spectrum of the same data showing only the evaporation residue (ER) and fission fragment (FF) intensities projected onto the time axis.

Self-supporting targets of ^{165}Ho, ^{197}Au, and ^{209}Bi with thicknesses of 400 μg/cm^2 were used. The absolute cross sections were obtained through normalization to elastic scattering measured in two monitor detectors positioned on the left and right sides of the beam at in-plane angles of $\theta=\pm5.2°$ and an out-of-plane angle of 11.1°. These monitor detectors were calibrated by measurements of Rutherford scattering at far forward angles by the two fragment detectors. The systematic errors are estimated to be 10% for the absolute cross sections and $\pm0.3°$ for the detector angle positions.

III. RESULTS AND DISCUSSION

A. Rotating-liquid-drop model

In Fig. 2 the experimental fission fragment angular distributions, normalized to one at $\theta_{\mathrm{c.m.}}=90°$, are compared with the theoretical predictions of the RLDM. These theoretical calculations require a knowledge of the I-dependent value of $K_0^2(I)$, which is a product of the effective moment of inertia $\mathcal{I}_{\mathrm{eff}}(I)$ [see Eq. (2)] at the shape where the K distribution is frozen in and the nuclear temperature T. On the right-hand side of Fig. 2 are shown the inverse effective moments of inertia, $\mathcal{I}_{\mathrm{sph}}/\mathcal{I}_{\mathrm{eff}}(I)$, predicted by the RLDM (Ref. 4) for the saddle point configuration as a function of I^2. The solid lines

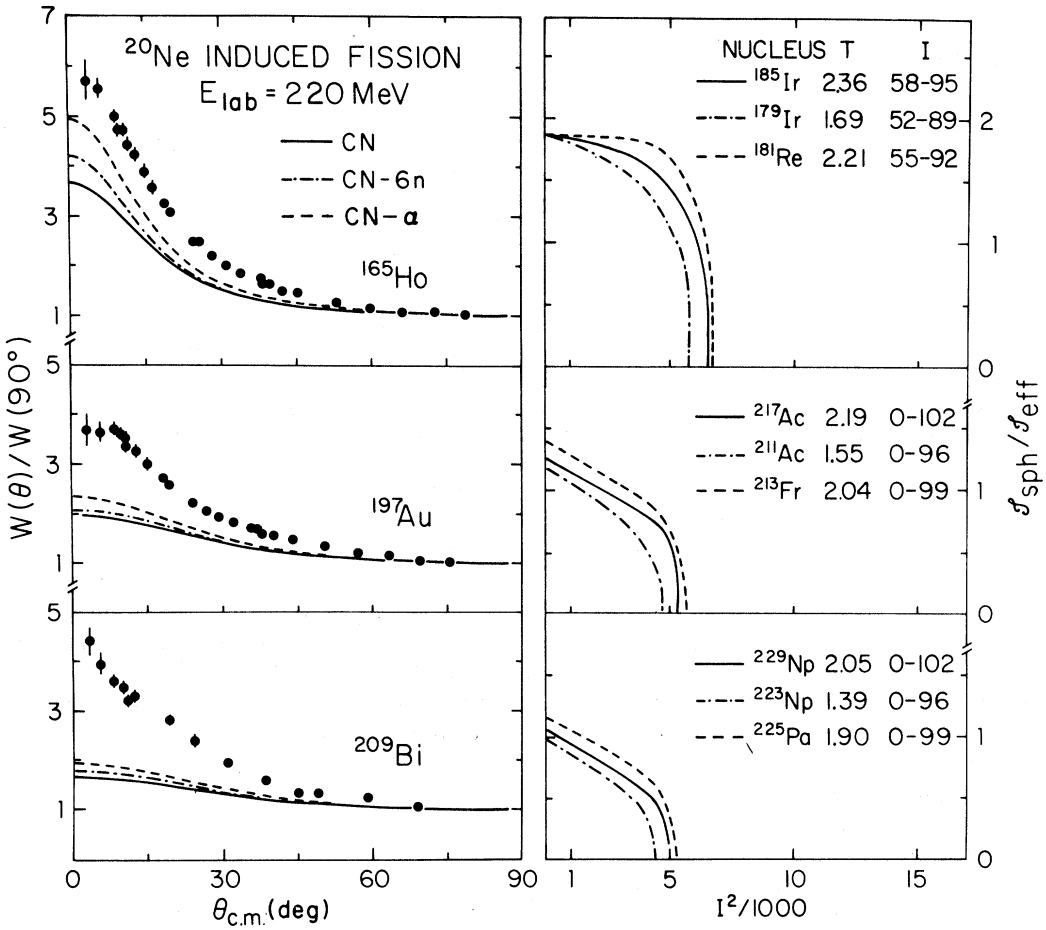

FIG. 2. Comparison of the experimental fission fragment angular distributions (points) with calculated results (lines) based on the rotating-liquid-drop model. The laboratory ^{20}Ne energy is 220 MeV for all reactions. The angular distributions (lines) on the left are calculated with the corresponding spin-dependent values of $\mathcal{I}_{sph}/\mathcal{I}_{eff}(I)$ shown on the right. The solid, dashed, and dashed-dotted curves correspond to the prefission emission of no particles, to one alpha particle, and to six neutrons, respectively. The nuclear temperature and I window applicable for each calculation are listed on the right-hand side and are discussed in the text.

represent the I-dependent saddle shapes of the respective compound nuclei. The dashed and dashed-dotted curves represent the effective moments of inertia of compound nuclei where one alpha particle or six neutrons, respectively, are emitted prior to fission.

The spin-dependent nuclear temperature at the appropriate nuclear shape where the K distribution is frozen in may be written as

$$T(K,I)=[(8/A)(E_{\text{c.m.}}+Q-B_f(I) -E^s_{\text{rot}}(K,I)-E_{\text{PP}})]^{1/2}, \quad (4)$$

where $B_f(I)$ is the fission barrier, $E^s_{\text{rot}}(K,I)$ is the rotational energy corresponding to the above nuclear shape, and E_{PP} is the energy removed by the prefission particles. Since the interpretation of calculations using Eq. (4) is complicated, the calculations presented in Sec. III utilize an approximate spin-independent nuclear temperature given by

$$T=[(8/A)(E_{\text{c.m.}}+Q-\langle E_{\text{rot}}\rangle-E_{\text{PP}})]^{1/2}, \quad (5)$$

where

$$\langle E_{\text{rot}}\rangle=\hbar^2\langle I^2\rangle/2\mathcal{I}_{\text{sph}}.$$

This is justified, as comparisons of angular distributions calculated with the nuclear temperatures defined by Eqs. (4) and (5) show no significant difference. The values of E_{PP} are assumed in the calculations to be 0, 20, and 68 MeV, respectively, for no prefission particles, one prefission alpha particle, and six prefission neutrons. Prefission particles also remove angular momentum. For simplicity it is assumed in all calculations that the spin of the compound nucleus is reduced by 3 and 6$\hbar$ by one prefis-

TABLE I. Summary of results for 220-MeV ^{20}Ne induced fission (see Sec. III C).

Target	X	σ_{ER} mb	σ_{FF} mb	l_{ER}	l_f	$\langle y\rangle$[a]	$K_0^2(I)$[b]	T MeV	$\frac{\mathcal{I}_{sph}}{\mathcal{I}_{eff}(I)}$[c]	$\frac{W(10°)}{W(90°)}$
^{165}Ho	0.663	620±60	1070±110	58	95	0.065	285±15	2.36	0.71	4.80±0.10
	0.674[d]					0.059	240±15[e]	1.69[f]	0.57	
^{197}Au	0.761	0	1900±190	0	102	0.038	400±40	2.19	0.62	3.50±0.15
	0.771[d]					0.035	330±30[e]	1.55[f]	0.50	
^{209}Bi	0.792	0	1850±185	0	102	0.034	400±30	2.05	0.63	3.50±0.10
	0.802[d]					0.030	335±25[e]	1.39[f]	0.49	

[a] $\langle y\rangle = 1.9249\langle I^2\rangle/\{1-1.7826[(N-Z)/A]^2\}A^{7/3}$.

[b] The best fit value $K_0^2(I)$ is assumed to be constant independent of I (see Sec. III B).

[c] $\mathcal{I}_{sph}$ is calculated with $r_0 = 1.2249F$, and $\mathcal{I}_{sph}/\mathcal{I}_{eff}(I)$ is a rectangular distribution independent of I.

[d] Based on the emission of six prefission neutrons.

[e] It is assumed that six prefission neutrons decrease the spin of the compound nucleus by $6\hbar$.

[f] Temperature determined from Eq. (4) assuming six prefission neutrons. In the case of the ^{165}Ho+^{20}Ne reaction, a temperature of 1.64 MeV has been measured from fission fragment neutron spectra (Ref. 7).

sion alpha particle and six prefission neutrons, respectively, as suggested by evaporation calculations. The removal of angular momentum also changes $\langle E_{rot}\rangle$ slightly. The nuclear temperature and I range appropriate in each calculation are shown on the right-hand side of Fig. 2.

The corresponding theoretical angular distributions are plotted on the left-hand side of Fig. 2 as calculated with the spin-dependent values of $K_0^2(I)$ resulting from the RLDM values of $\mathcal{I}_{eff}(I)$ displayed on the right-hand side of Fig. 2. The transmission coefficients required in Eq. (3) were assumed to be given by $T_I = 1$ for angular momenta in the range $l_{ER} \le I \le l_f$, and $T_I = 0$ for all other angular momenta. The values of l_{ER} and l_f are deduced from the evaporation residue (σ_{ER}) and fusion-fission (σ_{FF}) cross sections, respectively. All of these quantities are listed in Table I. The use of a smooth-cutoff model for T_I in Eq. (3) does not significantly change the results reported in the various subsections of Sec. III. When prefission particles are emitted, Eq. (3) has to be modified slightly with an additional normalization factor. Based on the comparisons of the calculations in this subsection with experimental data, one concludes that utilization of $\mathcal{I}_{sph}/\mathcal{I}_{eff}(I)$ values of the RLDM together with the assumption that $\mathcal{I}_{sph}/\mathcal{I}_{eff}(I)$ vanishes for $I > I_{RLDM}$ (where $B_f = 0$) gives angular distributions that are in marked disagreement with experiments.

B. Dependence of the fission fragment angular distribution on the functional form of $\mathcal{I}_{sph}/\mathcal{I}_{eff}(I)$

The sensitivity of the fission fragment angular distributions to the assumed functional relationship between $\mathcal{I}_{sph}/\mathcal{I}_{eff}(I)$ and I^2 is illustrated in Fig. 3. Four different dependences of $\mathcal{I}_{sph}/\mathcal{I}_{eff}(I)$ as a function of I^2 are shown in the insert of Fig. 3. The corresponding angular distributions based on these functions, a nuclear temperature of 1 or 2 MeV, and

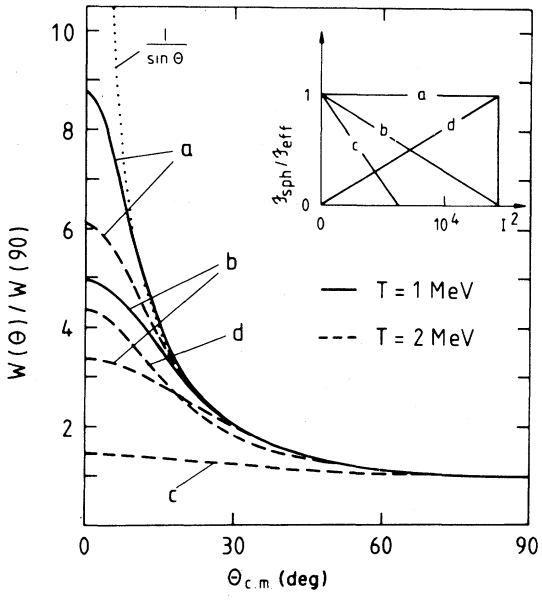

FIG. 3. Fission fragment angular distributions calculated with various assumed functional relationships between $\mathcal{I}_{sph}/\mathcal{I}_{eff}(I)$ and I^2. In all cases fission is assumed to occur for a nucleus with $A = 229$ and I values between 0 and 120, and a nuclear temperature of either 1.0 or 2.0 MeV. The limiting case of $W(\theta)/W(90°) \propto 1/\sin\theta$ corresponds to $\mathcal{I}_{sph}/\mathcal{I}_{eff} = \infty$, where $W(\theta)/W(90°) = 1$ corresponds to $\mathcal{I}_{sph}/\mathcal{I}_{eff} = 0$ (for all I).

a spin range of $0 \leq I \leq 120$, are shown also in this figure for a fissioning system with $A = 229$. One notices that the rectangular distribution labeled (a) with $T = 1$ MeV gives the largest anisotropy. As the temperature is increased to 2 MeV, the anisotropy decreases. The anisotropy scales inversely with the magnitude of $T/[\mathcal{I}_{\rm sph}/\mathcal{I}_{\rm eff}(I)]$. For example, the angular distribution for case (a) with a nuclear temperature of 1 MeV is identical to that for a rectangular distribution with $\mathcal{I}_{\rm sph}/\mathcal{I}_{\rm eff}(I) = 2$ and a nuclear temperature of 2 MeV. For the rectangular distribution (a) and a temperature of 1 MeV, the angular distribution follows a $1/\sin\theta$ distribution for all angles $\theta \geq 10°$. When the temperature is increased to 2 MeV, the angular distribution follows a $1/\sin\theta$ distribution for angles $\theta \geq 15°$. The triangular distribution (c) is somewhat similar to that of the RLDM for ^{229}Np and gives the smallest anisotropy. For the same nuclear temperature, distribution (d) gives a larger anisotropy than distribution (b), although distribution (d) leads to an angular distribution that deviates substantially from $1/\sin\theta$. Comparison between the fission fragment angular distributions for the $\mathcal{I}_{\rm sph}/\mathcal{I}_{\rm eff}(I)$ distributions (a), (b), and (d) can be more clearly seen in Fig. 4, where

$$d\sigma/d\theta \propto \sin\theta \cdot W(\theta)/W(90°)$$

is plotted as a function of θ. Here it can be inferred that distribution (d) gives a fission fragment angular distribution that deviates from $1/\sin\theta$ in a different way than distribution (b). As observed in Fig. 4, the function $\sin\theta \cdot W(\theta)/W(90°)$ never becomes larger than unity for distribution (d).

C. "Best fit" values of K_0^2

In this subsection each of the experimental fission fragment angular distributions is fitted with Eq. (3) by assuming a single I-independent value of $K_0^2(I)$.

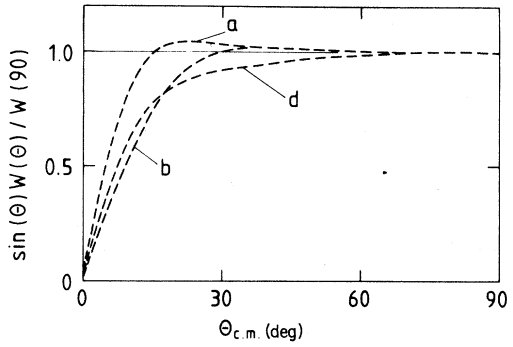

FIG. 4. Theoretical fission fragment angular distributions displayed as $d\sigma/d\theta \propto \sin\theta \cdot W(\theta)/W(90°)$ as a function of θ. Curves (a), (b), and (d) correspond to the $\mathcal{I}_{\rm sph}/\mathcal{I}_{\rm eff}(I)$ distributions shown in Fig. 2 and the parameters given in the caption of Fig. 2 with $T = 2$ MeV.

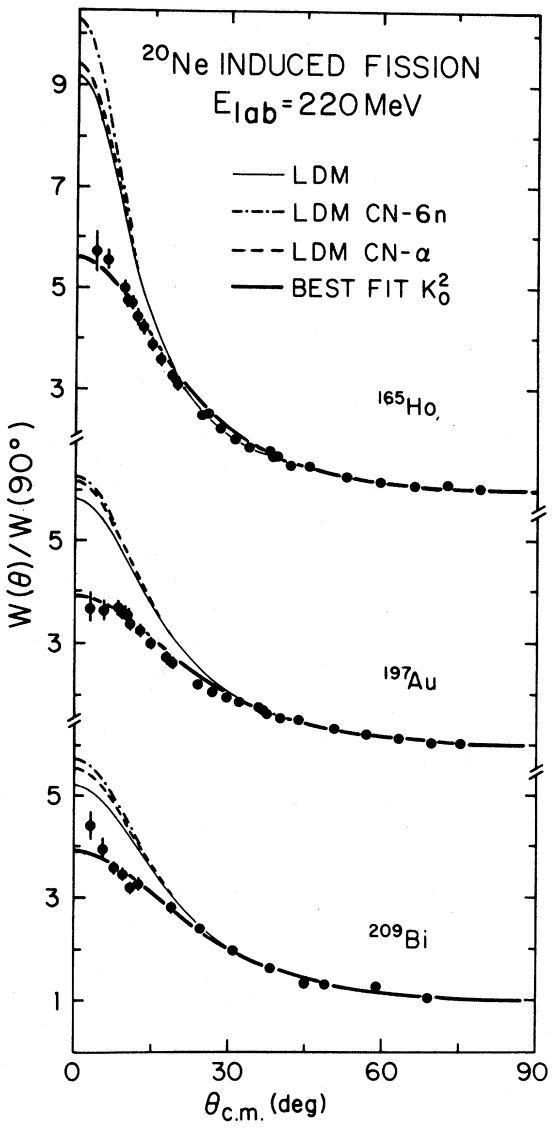

FIG. 5. Fission fragment angular distributions for 220-MeV ^{20}Ne-induced fission of ^{165}Ho, ^{197}Au, and ^{209}Bi targets. The experimental data are given by solid points and results of the various calculations are displayed by the lines. All calculations utilize a rectangular distribution of $\mathcal{I}_{\rm sph}/\mathcal{I}_{\rm eff}(I)$, where $\mathcal{I}_{\rm sph}/\mathcal{I}_{\rm eff}(I)$ is independent of I. The heavy solid line gives a best fit value of K_0^2 for the I window $l_{\rm ER} \leq I \leq l_f$ (see Table I for the change in K_0^2 when correction is made for the angular momentum removed by prefission particles). The thin solid line, dashed line, and dashed-dotted line give, respectively, the angular distributions based on the liquid-drop value of $\mathcal{I}_{\rm sph}/\mathcal{I}_{\rm eff}$ $(I = 0)$ for all I for the compound nucleus, the compound nucleus minus one prefission alpha particle, and the compound nucleus minus six prefission neutrons. For the cases of prefission particle emission, account is taken of the energy and angular momentum removed, as well as the change in $\mathcal{I}_{\rm sph}/\mathcal{I}_{\rm eff}$ $(I = 0)$.

Whether or not such a simple parametrization of the data is realistic is presently unknown. The above analysis is equivalent to a rectangular distribution of $\mathcal{I}_{\rm sph}/\mathcal{I}_{\rm eff}(I)$ discussed in Sec. III B. The I-independent parameter $K_0^2(I)$ and $\mathcal{I}_{\rm sph}/\mathcal{I}_{\rm eff}(I)$ are related through an appropriate nuclear temperature T [see Eq. (1)].

The "best fit" values of $K_0^2(I)$ giving the heavy solid lines in Fig. 5 are listed in Table I. The first entry for each target assumes that there are no prefission particles emitted. Hence, the limits on the I integration in Eq. (3) are $l_{\rm ER} \leq I \leq l_f$. In the second entry it is assumed that six prefission neutrons are emitted. The best fit values of K_0^2 are slightly altered due to the removal of angular momentum prior to fission. The six prefission neutrons are assumed to remove, in addition to the six units of angular momentum, 68 MeV of excitation energy. Therefore, the nuclear temperature, as calculated from Eq. (5) with $E_{\rm PP}$ and a slightly smaller value of $\langle E_{\rm rot} \rangle$, is reduced by some 30%.

In the case of the ^{165}Ho+^{20}Ne reaction ($E_{\rm lab}$=220 MeV), the nuclear temperature of the post-scission neutrons was measured[7] to be 1.64±0.33 MeV. This value is in good agreement with that calculated for fission fragments from Eq. (5). More importantly, the nuclear temperature applicable to the fissioning system, following the prefission emission of six neutrons, is calculated by Eq. (5) to be 1.69 MeV, a value nearly the same as that given previously.

In Fig. 5, the thin solid line, dashed line, and dashed-dotted line give, respectively, the fission fragment angular distribution based on the liquid-drop value of $\mathcal{I}_{\rm sph}/\mathcal{I}_{\rm eff}$ ($I=0$) for all I for the composite nucleus, the composite nucleus minus one prefission alpha particle, and the composite nucleus minus six prefission neutrons. For the cases where prefission particle emission occurs, the angular momentum and excitation energy are changed as discussed in Sec. III A. All of the above theoretical calculations that utilize nonrotating liquid-drop values of $\mathcal{I}_{\rm sph}/\mathcal{I}_{\rm eff}$ ($I=0$) give anisotropies that are larger than the experimental values.

In order to obtain the best fit heavy solid lines in Fig. 5, the K distribution must be frozen in at a more compact configuration than that of the nonrotating liquid drop model. These configurations are reported in Table I in terms of the parameter $\mathcal{I}_{\rm sph}/\mathcal{I}_{\rm eff}(I)$, where the analysis is based on a constant value of $\mathcal{I}_{\rm sph}/\mathcal{I}_{\rm eff}(I)$ *independent* of I. As can be seen by comparing the two entries in Table I, the presence of prefission particle emission markedly changes the determined value of $\mathcal{I}_{\rm sph}/\mathcal{I}_{\rm eff}(I)$ (however, see Sec. III E for additional effects associated with prefission particles).

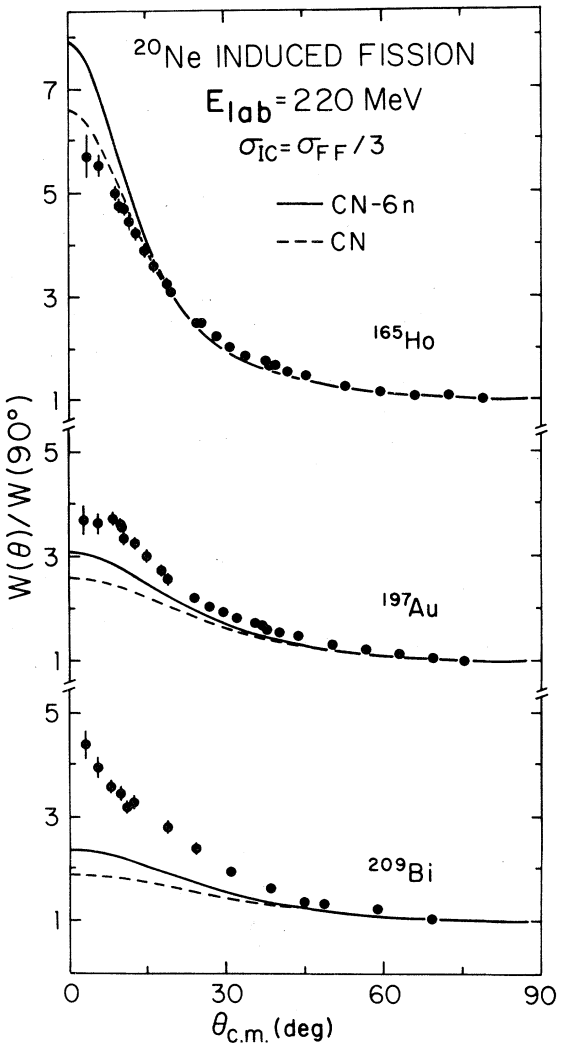

FIG. 6. Comparison of experimental fission fragment angular distributions (points) with calculated results (lines) based on the rotating-liquid-drop model and the assumption that one-third of the fission cross section is due to incomplete fusion (see text). The solid and dashed line, respectively, correspond to six prefission neutrons and no prefission particles.

D. Incomplete projectile fusion

Some of the conclusions reached in previous subsections are true only if the spin distribution of the composite nuclei is identical to that of the initial orbital angular momentum as deduced from the cross sections listed on Table I. This is, of course, not true for incomplete fusion where the projectile undergoes prefusion breakup and only part of the projectile fuses with the target. The emitted breakup particle of mass m carries away both energy and angular momentum.[14] For example, the loss of angular momentum Δl is assumed to be given by

$\Delta l = (m/m_p)\cdot l$, where m_p is the projectile mass.

For the three reactions discussed here, however, at a somewhat higher bombarding energy of 292 MeV, Tubbs *et al.*[15] determined the contribution of incomplete fusion by means of fission fragment-fission fragment angular correlation measurements. At this energy the contribution of events with incomplete linear momentum transfer is of the order of 40% of the total fission cross section. In order to investigate the effect of incomplete fusion on the calculated fission fragment angular distributions, the following simplifying assumptions have been made:

(a) One-third of the fusion-fission cross section is due to incomplete fusion; furthermore, this cross section originates from ^{16}O capture.

(b) Incomplete fusion arises from the highest partial waves l_i.

(c) The spins of the composite nuclei populated by incomplete fusion are calculated from the relation

$$I_{If} = \left[1 - \frac{m}{m_p}\right]\cdot l_i = \left(\tfrac{16}{20}\right)\cdot l_i \ ,$$

where l_i are the initial angular momenta in the l window making up the total incomplete-fusion cross section.

(d) The partial cross section for each spin I_{If} is proportional to the corresponding weighting factor $2l_i+1$.

(e) The nuclear temperature is adjusted to account for the new center-of-mass energy $(\frac{16}{20})E_{\text{c.m.}}(^{20}\text{Ne})$ and Q value.

(f) The values of $\mathcal{I}_{\text{sph}}/\mathcal{I}_{\text{eff}}(I)$ for incomplete and complete fusion are those of the RLDM for fission of a composite system with and without emission of one prefission alpha particle, respectively, as shown by the dashed and solid curves on the right-hand side of Fig. 2.

Theoretical fission fragment angular distributions obtained by incorporating incomplete fusion into the calculations, as described above, are shown in Fig. 6. These results are to be compared to the previous RLDM fission fragment angular distributions plotted in Fig. 2. Two calculations are performed for each target, one calculation without prefission particles and one with six prefission neutrons. For example, with a ^{165}Ho target and no prefission particle emission, the fissioning nuclei are

^{185}Ir ($T=2.41$ MeV, $58 \le I \le 84$)

and

^{181}Re ($T=2.08$ MeV, $85 \le l \le 95 \Rightarrow 68 \le I \le 76$) .

With six prefission neutrons, the fissioning nuclei are

^{179}Ir ($T=1.76$ MeV, $58 \le l \le 84 \Rightarrow 52 \le I \le 78$)

and

^{175}Re ($T=1.22$ MeV, $85 \le l \le 95 \Rightarrow 68 \le I' \le 76 \Rightarrow 62 \le I \le 71$) .

In the application of Eq. (3), in order to obtain the correct cross section, the above four spin distributions require normalization factors of 1,

$$\tfrac{5}{4}[(\tfrac{5}{2})I+1]/(2I+1) \ ,$$

$$(2l+1)/(2I+1) \ ,$$

and

$$\tfrac{5}{4}[(\tfrac{5}{2})I'+1]/(2I+1) \ ,$$

respectively.

If one-third of the fission cross section is due to incomplete fusion, the theoretical anisotropy for the RLDM increases in the direction of the experimental data. However, the increase is small for the two more fissile systems, and it requires unrealistically large incomplete-fusion contributions in order to obtain a fit to the angular distributions. This is due to the fact that a large number of the reduced spin values associated with incomplete fusion still exceed I_{RLDM} ($B_f=0$). In the case of the ^{165}Ho+^{20}Ne system, the theoretical cross section increases considerably at small angles and qualitative agreement with the data is obtained when no prefission neutrons are included. With six prefission neutrons the theoretical anisotropy becomes too large for the ^{165}Ho+^{20}Ne system.

E. Effect of dealignment of composite nuclei due to prefission neutron emission

In the derivation of Eq. (3), it has been assumed that all spins of the composite nuclei are aligned in a plane perpendicular to the beam direction which is chosen as the Z axis. This is equivalent to the assumption that $M=0$. Although the spin of the ^{20}Ne projectile is zero, the ground-state spins of the

^{165}Ho, ^{197}Au, and ^{209}Bi targets are $\frac{7}{2}^-$, $\frac{3}{2}^+$, and $\frac{9}{2}^-$, respectively. Consequently, the assumption that $M=0$ is not exactly fulfilled. A much more important effect than that of target spin on the invalidation of the assumption that $M=0$, however, is the emission of light particles from the recoiling composite nuclei prior to fission. With prefission particle emission, one must sum over all possible M substates weighted with the M population $P(M,I)$ at the moment of fission. Unfortunately, one does not know this population function. However, it is possible to approximate the M summation by averaging the fission angular distributions over an angular range corresponding to the dealignment of the spin axis. The angle,

$$\langle\theta\rangle \approx \tan^{-1}(\langle\, |M|\, \rangle/\langle I\rangle)\ ,$$

is approximately 5° in the present experiment if one assumes that six neutrons are emitted prior to fission. The effective dealignment of the Z axis has been approximated by the angular distribution function

$$P(\theta)=\exp\{-0.123\theta-0.00364\theta^2\}\ , \tag{6}$$

where θ is expressed in degrees. This function [Eq. (6)] has been folded with the theoretical angular distribution of fission fragments given by Eq. (3) yielding the following relation:

$$\frac{d\sigma}{d\Omega_{\rm FF}}(\theta_{\rm FF})=\frac{\int_\nu\int_\phi \frac{dP}{d\Omega}[\epsilon(\nu,\phi)]\frac{d\sigma}{d\Omega_{\rm FF}}(\theta_{\rm FF}-\epsilon)\sin\nu\, d\nu\, d\phi}{\int_\nu\int_\phi \frac{dP}{d\Omega}[\epsilon(\nu,\phi)]\sin\nu\, d\nu\, d\phi}\ , \tag{7}$$

where ϵ is the angle between the direction (ν,ϕ) and the fission fragment direction of flight $(\theta_{\rm FF},\Phi_{\rm FF}=0)$. In the application of Eq. (7) the ν integration is carried out over the angular range $0°\le\nu\le 30°$, where $P(\theta)$ varies more than three orders of magnitude, and the ϕ integration is over 2π.

The results of theoretical calculations of fission fragment angular distributions where account is taken of the dealignment of the spin vectors of the composite nuclei are tabulated in Table II and

TABLE II. Effect of dealignment of the angular momentum due to six prefission neutrons.

Target	Fissioning nucleus	X	I window	Model	K_0^2	T MeV	$\mathcal{I}_{\rm sph}/\mathcal{I}_{\rm eff}(I)$	Line in Fig. 7
^{165}Ho	^{179}Ir	0.674	$52\le I\le 89$	best fit	160±15	1.69	0.86	heavy solid
^{197}Au	^{211}Ac	0.771	$0\le I\le 96$	best fit	260±30	1.55	0.64	heavy solid
^{209}Bi	^{223}Np	0.802	$0\le I\le 96$	best fit	260±25	1.39	0.63	heavy solid
^{165}Ho	^{179}Ir	0.674	$52\le I\le 89$	LMD ($I=0$)	75.0	1.69	1.84	dashed
^{197}Au	^{211}Ac	0.771	$0\le I\le 96$	LDM ($I=0$)	140.0	1.55	1.19	dashed
^{209}Bi	^{223}Np	0.802	$0\le I\le 96$	LDM ($I=0$)	165.3	1.39	0.99	dashed
^{165}Ho	^{179}Ir	0.674	$52\le I\le 89$	RLDM	(I dependent)	1.69	I dependent	dashed-dotted
^{197}Au	^{211}Ac	0.771	$0\le I\le 96$	RLDM	(I dependent)	1.55	I dependent	dashed-dotted
^{209}Bi	^{223}Np	0.802	$0\le I\le 96$	RLDM	(I dependent)	1.39	I dependent	dashed-dotted
^{165}Ho	^{179}Ir	0.674	$52\le I\le 78$	best fit with 33%	140±15	1.76	0.91[a]	not plotted
	^{175}Re	0.656	$62\le I\le 71$	incomplete fusion		1.22		
^{197}Au	^{211}Ac	0.771	$0\le I\le 77$	best fit with 33%	240±20	1.64	0.66[a]	not plotted
	^{207}Fr	0.753	$61\le I\le 76$	incomplete fusion		1.15		
^{209}Bi	^{223}Np	0.802	$0\le I\le 77$	best fit with 33%	240±20	1.48	0.62[a]	not plotted
	^{219}Pa	0.783	$61\le I\le 76$	incomplete fusion		0.85		

[a]Calculated with the expression $\langle\mathcal{I}_{\rm sph}/\mathcal{I}_{\rm eff}(I)\rangle=[\frac{2}{3}(\mathcal{I}_{\rm sph}T/\hbar^2)_A+\frac{1}{3}(\mathcal{I}_{\rm sph}T/\hbar^2)_{A-4}]/K_0^2$.

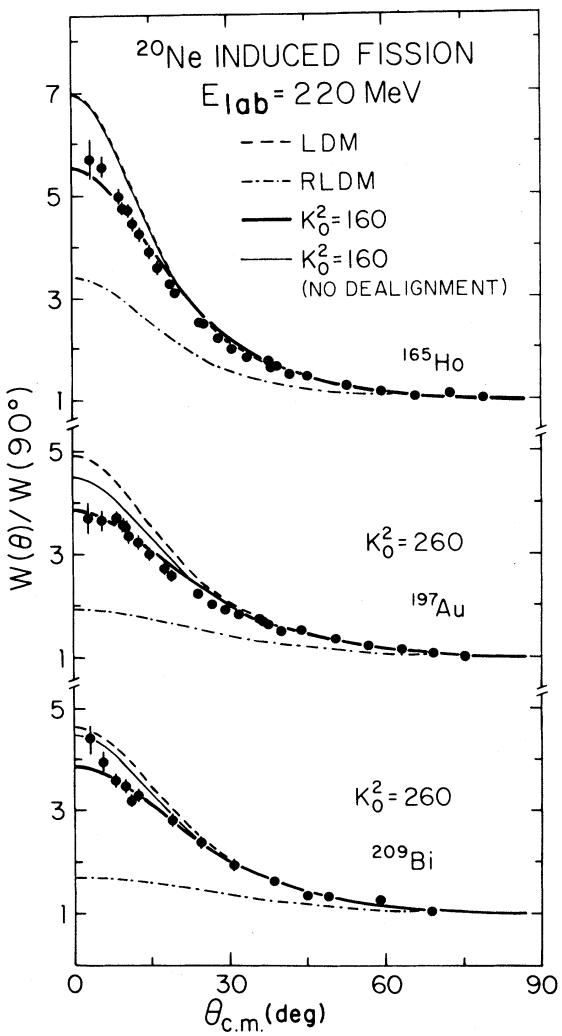

FIG. 7. Effect of dealignment of prefission recoil nuclei (due to six prefission neutrons) on the experimental fission fragment angular distribution. Four curves are included for each reaction, three of which take account of the dealignment of the prefission recoil nuclei. The heavy solid line leads to the best fit value of K_0^2 listed in Table II. The thin solid line utilizes this K_0^2 value, but, however, neglects the dealignment effect. The dashed and dashed-dotted lines represent calculations with the non rotating [$\mathcal{I}_{sph}/\mathcal{I}_{eff}$ ($I=0$)] LDM and RLDM calculations, respectively. (See text and Table II.)

shown in Fig. 7. In all of the computations, it is assumed that six neutrons are emitted prior to fission. As discussed previously, these prefission neutrons reduce both the temperature and spin of the composite nucleus prior to fission. The best fit value of K_0^2 listed in Table II for each target leads to the heavy solid line in Fig. 7. If the folding is neglected and K_0^2 is kept the same as that deduced from the fit that gives the heavy solid line in Fig. 7, the thin solid line results. Hence, the effect of the dealignment is to reduce the anisotropy. The magnitude of the effect calculated with the folding function given by Eq. (6) is estimated to be an upper limit for the real effect. The dashed and dashed-dotted curves in Fig. 7 represent the theoretical angular distributions, including the dealignment effect, for the LDM ($I=0$) and the RLDM, respectively. The LDM gives too large an anisotropy, whereas the RLDM underestimates the anisotropy.

Included also in Table II is the best fit value of K_0^2 for each target when incomplete fusion makes up one-third of the total fusion-fission cross section. When account is taken of incomplete fusion in the calculations, the derived best fit value of K_0^2 is reduced by approximately 10%.

F. Angular distributions with spin dependent values of $\mathcal{I}_{sph}/\mathcal{I}_{eff}(I)$

As can be seen from Figs. 2, 6, and 7 the RLDM predicts fission-fragment anisotropies that are far too small, except for the ^{165}Ho+^{20}Ne reaction, when it is assumed that one-third of the fission cross section is due to incomplete fusion (see Fig. 6). However, even with the latter assumption the theoretical anisotropies are too small for the more fissile ^{197}Au+^{20}Ne and ^{209}Bi+^{20}Ne systems.

It is possible, however, to obtain reasonable fits to the experimental fission fragment angular distributions with spin dependent values of $\mathcal{I}_{sph}/\mathcal{I}_{eff}(I)$ if one relaxes the criterion of the RLDM that $\mathcal{I}_{sph}/\mathcal{I}_{eff}(I)=0$ when $I>I_{RLDM}$ (where $B_f=0$). Theoretical calculations have been performed with different functional dependences of $\mathcal{I}_{sph}/\mathcal{I}_{eff}(I)$ on I. Two of these are as follows:

(1) $\mathcal{I}_{sph}/\mathcal{I}_{eff}(I)$ is equal to

$$[\mathcal{I}_{sph}/\mathcal{I}_{eff}(I=0)]_{RLDM}$$

for $I=0$, and decreases linearly with I^2, becoming zero for $I \geq l_f$.

(2) The RLDM functional form of $\mathcal{I}_{sph}/\mathcal{I}_{eff}(I)$ is scaled such that $\mathcal{I}_{sph}/\mathcal{I}_{eff}(I)$ goes to zero for $I=l_f$ rather than $I=I_{RLDM}$ (where $B_f=0$). This is accomplished by letting

$$\mathcal{I}_{sph}/\mathcal{I}_{eff}(I'^2)=[\mathcal{I}_{sph}/\mathcal{I}_{eff}(I^2)]_{RLDM} ,$$

where

$$I'^2=[l_f^2/I_{RLDM}^2(B_f=0)]I^2 .$$

The functional forms of $\mathcal{I}_{sph}/\mathcal{I}_{eff}(I)$ vs I^2 described in the above assumption (1) in Eq. (1) are shown on the right-hand side of Fig. 8. These curves are quite similar to what is obtained when one extrapolates the $[\mathcal{I}_{sph}/\mathcal{I}_{eff}(I)]_{RLDM}$ function

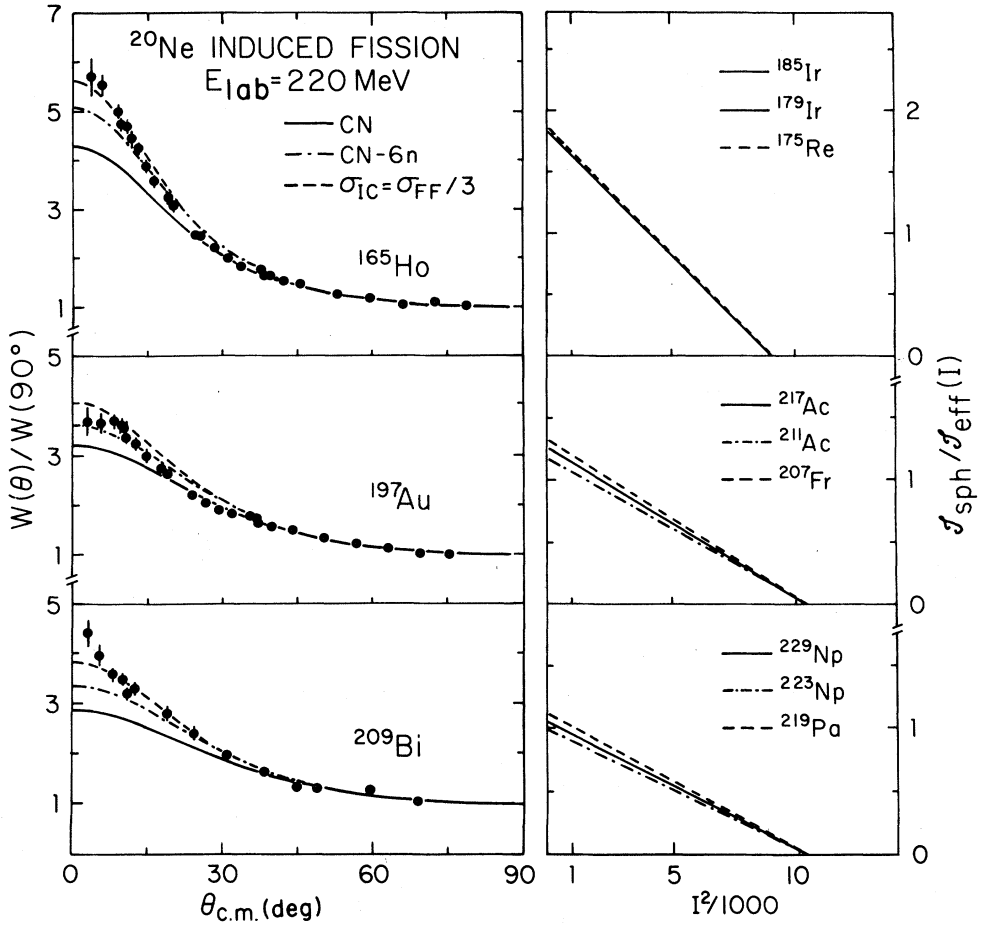

FIG. 8. Comparison of experimental fission fragment angular distributions with theory based on spin dependent values of $\mathcal{I}_{sph}/\mathcal{I}_{eff}(I)$. The functional forms of $\mathcal{I}_{sph}/\mathcal{I}_{eff}(I)$ are shown on the right-hand side. The three theoretical curves, shown on the left-hand side along with the data (solid points), are for no prefission particle emission (solid line), emission of six prefission neutrons (dashed-dotted line), and one-third of the fission cross section due to incomplete fusion as well as the emission of six prefission neutrons (dashed line).

from I^2 values just below the sharp bend out to $I^2=I_f^2$ (see the right-hand side of Fig. 2). The theoretical fission fragment angular distributions shown on the left-hand side of Fig. 8 are for no prefission particle emission (solid curve), six prefission neutrons (dashed-dotted curve), and one-third of the fission cross section due to incomplete fusion as well as six prefission neutrons (dashed curve). As can be seen in Fig. 8, the theoretical fission fragment angular distributions calculated with the functional forms of $\mathcal{I}_{sph}/\mathcal{I}_{eff}(I)$ shown on the right-hand side of Fig. 8 give rather good fits to the experimental data for the cases where six prefission neutrons are emitted (dashed-dotted line), and one-third of the fission cross section is due to incomplete fusion as well as the emission of six prefission neutrons (dashed line). Slightly altering the distributions on the right-hand side of Fig. 8 will give an even better fit to the data. The theoretical anisotropies calculated with the functional form of $\mathcal{I}_{sph}/\mathcal{I}_{eff}(I)$ described in the above assumption (2) are approximately 10% too large, and are not shown in Fig. 8.

G. Comparison of results with the nonrotating ($I=0$) liquid drop model

In Sec. III C and III E four best fit values of K_0^2 are determined from each experimental fission fragment angular distribution. The four values of K_0^2 (see Tables I and II) correspond to (a) no prefission particle emission, (b) emission of six prefission neutrons, (c) emission of six prefission neutrons along with an approximate correction for spin dealign-

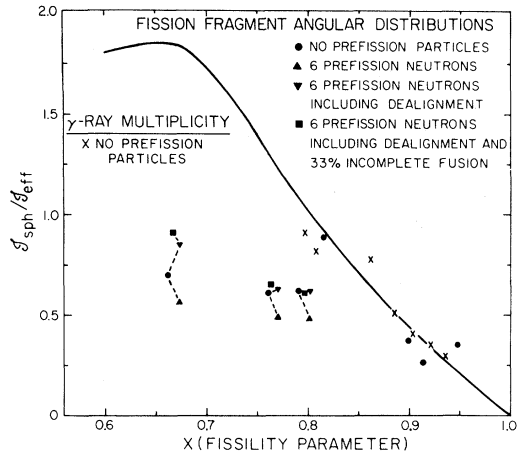

FIG. 9. Comparison of the *spin independent* experimental values of $\mathcal{I}_{sph}/\mathcal{I}_{eff}$ determined from heavy-ion reactions with the nonrotating liquid drop model. The solid line represents the theoretical nonrotating liquid drop model values of $\mathcal{I}_{sph}/\mathcal{I}_{eff}$ $(I=0)$ as a function of the fissibility parameter

$$X=(Z^2/A)/50.883\{1-1.7826[(N-Z)/A]^2\} .$$

The three groups of four points each are based on the present work [each of the four points is based on the different assumptions (a)–(d) listed in Sec. III G]. The four single solid points are from Ref. 9 and the seven crosses from Ref. 16.

ment, and (d) emission of six prefission neutrons including spin dealignment and 33% incomplete fusion. Each of these K_0^2 values has been converted to a value of $\mathcal{I}_{sph}/\mathcal{I}_{eff}$ with Eq. (1) by utilizing the appropriate nuclear temperature T calculated with Eq. (5). The resulting four values of $\mathcal{I}_{sph}/\mathcal{I}_{eff}$ calculated from the fragment angular distributions of ^{20}Ne induced fission on each of the targets ^{165}Ho, ^{197}Au, and ^{209}Bi are plotted in Fig. 9. For each of the above assumptions (a)–(d), the I-independent value of $\mathcal{I}_{sph}/\mathcal{I}_{eff}$ deduced from the best fit values of K_0^2 is considerably smaller than the nonrotating liquid drop model value of $\mathcal{I}_{sph}/\mathcal{I}_{eff}$ $(I=0)$. This is true for all three ^{20}Ne induced reactions where the available energy above the Coulomb barrier $[(E_{c.m.}-V_{Coul})/\mu]$ ranges from 4.4 to 5.7 MeV per nucleon.

Fission fragment angular distributions[9] analyzed in a similar way for ^{32}S induced fission with targets of ^{197}Au, ^{232}Th, ^{238}U, and ^{248}Cm have yielded spin-independent values of $\mathcal{I}_{sph}/\mathcal{I}_{eff}$ nearly equal to those of the nonrotating liquid drop model values, i.e., $\mathcal{I}_{sph}/\mathcal{I}_{eff}$ $(I=0)$. The four values of $\mathcal{I}_{sph}/\mathcal{I}_{eff}$ plotted in Fig.9 as solid points are from Ref. 9. The ^{32}S induced fission differs from the ^{20}Ne induced fission in at least one important way, namely, the available energy above the Coulomb barrier is very small for the former reaction where $(E_{c.m.}-V_{Coul})/\mu$ ranges from 0.2 to 0.9 MeV per nucleon.

The spin-independent values of $\mathcal{I}_{sph}/\mathcal{I}_{eff}$ plotted as crosses in Fig. 9 are derived from γ ray multiplicity measurements reported by Bock *et al.*[16] In this method K_0^2 is assumed to be given by:[16]

$$K_0^2=\langle j\rangle^2-\langle l_z\rangle^2 , \tag{8}$$

where $\langle j\rangle=2(\langle M_\gamma\rangle-6)$, $\langle l_z\rangle=(\frac{4}{21})l_f$, $\langle M_\gamma\rangle$ is the measured average γ ray multiplicity, and l_f is calculated from the fusion-fission cross section employing a sharp-cutoff model. Equation (8) is thought to be valid for $l_f>60$. The reported[16] spin-independent values of $\mathcal{I}_{sph}/\mathcal{I}_{eff}$ $(I=0)$ determined by this technique are nearly the same as those calculated for the nonrotating liquid drop model.

There is an important difference in the present results obtained from energetic ^{20}Ne induced fission and the earlier results[9,16] obtained at lower energies above the Coulomb barrier. As can be seen in Fig. 9, the I-independent values of $\mathcal{I}_{sph}/\mathcal{I}_{eff}$ deduced from the ^{20}Ne induced fission are approximately only one-half those predicted by the nonrotating $(I=0)$ liquid drop model. In contrast to this, the earlier reported values[9,16] of $\mathcal{I}_{sph}/\mathcal{I}_{eff}$ are in good agreement with the liquid drop model. It is interesting to note that if the results from the ^{20}Ne induced fission are interpreted with a constant value of K_0^2, one concludes that the K distribution is frozen in at a much more compact configuration than predicted by the LDM.

IV. CONCLUSIONS

The experimental fission fragment angular distributions measured for 220-MeV ^{20}Ne induced fission of ^{165}Ho, ^{197}Au, and ^{209}Bi cannot be reproduced with either the rotating (RLDM) or nonrotating (LDM) liquid drop models. The former model produces an anisotropy that is too small, while the latter model leads to an anisotropy that is too large.

The *spin-independent* values of $\mathcal{I}_{sph}/\mathcal{I}_{eff}$ decrease by approximately 20% when the theory accounts for the energy and angular momentum removed by six prefission neutrons. If, however, the dealignment of the angular momentum produced by the prefission neutrons is also taken into account, the deduced values of $\mathcal{I}_{sph}/\mathcal{I}_{eff}$ increase again to values comparable to or slightly larger than those based on no prefission emission. Inclusion of 33% incomplete fusion slightly increases the values of $\mathcal{I}_{sph}/\mathcal{I}_{eff}$. Spin-independent values of $\mathcal{I}_{sph}/\mathcal{I}_{eff}$ deduced for the above three reactions are rather insensitive to prefission neutron emission and have values of about

50% of the LDM value of $\mathcal{I}_{\rm sph}/\mathcal{I}_{\rm eff}$ $(I=0)$ (see Tables I and II and Fig. 9).

It is possible to obtain satisfactory fits to the experimental fission fragment angular distributions with spin dependent values of $\mathcal{I}_{\rm sph}/\mathcal{I}_{\rm eff}(I)$ if the rotating liquid drop model condition that $\mathcal{I}_{\rm sph}/\mathcal{I}_{\rm eff}(I)$ goes to zero at $I_{\rm RLDM}$ $(B_f=0)$ is relaxed. For example, if $\mathcal{I}_{\rm sph}/\mathcal{I}_{\rm eff}(I)$ is equal to

$$[\mathcal{I}_{\rm sph}/\mathcal{I}_{\rm eff}(I=0)]_{\rm RLDM}$$

for $I=0$ and decreases linearly as a function of I^2 becoming zero for $I \geq l_f$, the data are reasonably well reproduced with such a functional form of $\mathcal{I}_{\rm sph}/\mathcal{I}_{\rm eff}(I)$. For reaction systems with large angular momenta, where the fission barrier has vanished, the stage at which the K distribution is frozen in may be near the turning point (or at a slightly later stage) of the trajectory, where it spends a considerable fraction of its lifetime.

The interpretation of fission fragment angular distributions in terms of moments of the K distribution presented in this paper makes extensive use of the functional relation between the variance $K_0{}^2$, the effective moment of inertia of the fissioning nucleus and the nuclear temperature, as given by Eq. (1). This relation, however, is valid only in the limit that the system is in a thermodynamic equilibrium with collective degrees of freedom that vary slowly, up to a point, from whereon the motion suddenly becomes highly nonadiabatic, effecting a freezing-in of the statistical K distribution. It is conceivable that, in reality, the change in collective velocities is much more gradual, leading to a dynamical evolution of the K distribution during the fission process, which is not well characterized by equilibrium-statistical theory. Depending on the results of a realistic dynamic modeling of the fission process, the present results could be subject to a later reinterpretation.

ACKNOWLEDGMENTS

This work was supported by the U.S. Department of Energy. Support was also provided by the Office of Naval Research under Contract N00014-76-C-0001 with the Center for Naval Analyses of the University of Rochester. One of us (D.H.) wants to thank the Rochester Group for their kind hospitality during the summer of 1982 when part of this work was done.

---

*Permanent address: Rudjar Bošković Institute, Zagreb, Yugoslavia.

[1]R. Vandenbosch and J. R. Huizenga, *Nuclear Fission* (Academic, New York, 1973).

[2]A. Bohr, *Proceedings of the United Nations International Conference on the Peaceful Uses of Atomic Energy* (United Nations, New York, 1956), Vol. 2, p. 151.

[3]R. F. Reising, G. L. Bate, and J. R. Huizenga, Phys. Rev. 141, 1161 (1966).

[4]S. Cohen, F. Plasil, and W. J. Swiatecki, Ann. Phys. (N.Y.) 82, 557 (1974).

[5]I. Halpern and V. M. Strutinsky, *Proceedings on the Second United Nations International Conference on the Peaceful Uses of Atomic Energy* (United Nations, New York, 1958), Vol. 15, p. 408.

[6]J. R. Huizenga, A. N. Behkami, and L. G. Moretto, Phys. Rev. 177, 1826 (1969).

[7]E. Holub, D. Hilscher, U. Jahnke, H. Orf, H. Rossner, and G. Ingold, *Proceedings of the 3rd International Conference on Nuclear Reaction Mechanisms, Varenna, 1982,* edited by E. Gadioli (University of Milano, Milano, 1982), Suppl. 28, p. 384.

[8]J. R. Birkelund, L. E. Tubbs, J. R. Huizenga, J. N. De, and D. Sperber, Phys. Rep. 56, 107 (1979).

[9]B. B. Back, H. G. Clerc, R. R. Betts, B. G. Glagola, and B. D. Wilkins, Phys. Rev. Lett. 46, 1068 (1981).

[10]J. Blocki, J. Randrup, W. J. Swiatecki, and C. F. Tsang, Ann. Phys. (N.Y.) 105, 477 (1977).

[11]J. Randrup, Ann. Phys. (N.Y.) 112, 356 (1978).

[12]W. J. Swiatecki, Phys. Scr. 24, 113 (1981).

[13]W. J. Swiatecki, Nucl. Phys. A376, 275 (1982).

[14]K. Siwek-Wilczynska, E. H. du Marchie van Voorthuysen, J. Van Popta, R. H. Siemssen, and J. Wilczyński, Phys. Rev. Lett. 42, 1599 (1979).

[15]L. E. Tubbs, J. R. Birkelund, J. R. Huizenga, W. W. Wilcke, D. Hilscher, B. Gebauer, H. Lettau, U. Jahnke, and H. Rossner (unpublished).

[16]R. Bock, Y. T. Chu, M. Dakowski, A. Gobbi, E. Grosse, A. Olmi, H. Sann, D. Schwalm, U. Lynen, W. Müller, S. Bjørnholm, H. Esbensen, W. Wölfli, and E. Morenzoni, Nucl. Phys. A388, 334 (1982).